Anthropogenic and Natural Contributions to the Lengthening of the Summer Season in the Northern Hemisphere

BO-JOUNG PARK, YEON-HEE KIM, AND SEUNG-KI MIN

Division of Environmental Science and Engineering, Pohang University of Science and Technology, Pohang, Gyeongbuk, South Korea

EUN-PA LIM

Bureau of Meteorology, Melbourne, Victoria, Australia

(Manuscript received 26 September 2017, in final form 10 April 2018)

ABSTRACT

Observed long-term variations in summer season timing and length in the Northern Hemisphere (NH) continents and their subregions were analyzed using temperature-based indices. The climatological mean showed coastal–inland contrast; summer starts and ends earlier inland than in coastal areas because of differences in heat capacity. Observations for the past 60 years (1953–2012) show lengthening of the summer season with earlier summer onset and delayed summer withdrawal across the NH. The summer onset advance contributed more to the observed increase in summer season length in many regions than the delay of summer withdrawal. To understand anthropogenic and natural contributions to the observed change, summer season trends from phase 5 of the Coupled Model Intercomparison Project (CMIP5) multimodel simulations forced with the observed external forcings [anthropogenic plus natural forcing (ALL), natural forcing only (NAT), and greenhouse gas forcing only (GHG)] were analyzed. ALL and GHG simulations were found to reproduce the overall observed global and regional lengthening trends, but NAT had negligible trends, which implies that increased greenhouse gases were the main cause of the observed changes. However, ALL runs tend to underestimate the observed trend of summer onset and overestimate that of withdrawal, the causes of which remain to be determined. Possible contributions of multidecadal variabilities, such as Pacific decadal oscillation and Atlantic multidecadal oscillation, to the observed regional trends in summer season length were also assessed. The results suggest that multidecadal variability can explain a moderate portion (about ±10%) of the observed trends in summer season length, mainly over the high latitudes.

1. Introduction

The seasonal cycle of Earth's climate influences the basic ecosystem functions, agricultural practices, and environmental–social characteristics of a given region (Walther et al. 2002; Parmesan 2006). Observed changes to seasonal cycles under climate change have become an important topic of interest because of their socioeconomic and ecological impacts (Bertram et al. 2001). Many researchers have investigated observed changes in the seasonal cycle in terms of phase and amplitude (Mann and Park 1996; Wallace and Osborn 2002; Stine et al. 2009; Dwyer et al. 2012; Qian and Zhang 2015; Cornes et al. 2017).

Mann and Park (1996) compared the observed changes in the amplitude and phase of the seasonal cycle with those from model simulations. They found that models could reproduce the observed decrease in the amplitude of the seasonal cycle in the Northern Hemisphere (NH), which was attributed to decreased winter ice cover caused by greenhouse warming. For changes in the phase of the seasonal cycle, models predicted a phase delay with time, in contrast to the phase advance in the observations, which was suggested to be caused in part by natural variability. Extending the work of Mann and Park (1996), Wallace and Osborn (2002) also compared the observed amplitude reduction in the seasonal cycle with simulated changes and found better agreement of the observations with greenhouse gas forcing when sulfate aerosol forcing, which has a cooling effect, was included.

Dwyer et al. (2012) identified latitudinal differences in model responses, which showed different phase trends from the observations. Because of sea ice loss, the increased heat capacity on the surface layer induced phase delay at high latitudes, whereas a small phase delay at

Corresponding author: Seung-Ki Min, skmin@postech.ac.kr

DOI: 10.1175/JCLI-D-17-0643.1

lower latitudes was expected, which is controlled by surface heat flux changes. Qian and Zhang (2015) examined regional changes in the amplitude of the annual cycle of temperatures at mid- to high latitudes over NH land and detected anthropogenic signals in the amplitude decrease in the annual cycle over many regions. Recently, analyzing long-term changes throughout the twentieth century, Cornes et al. (2017) found that external forcings alone cannot explain the observed change in the annual cycle amplitude, suggesting the important role of large-scale atmospheric variability.

Changes in the seasonal cycle can also be quantified by seasonal indicators (e.g., Stine et al. 2009) or through threshold-crossing statistics (e.g., Christidis et al. 2007; Qian et al. 2012). Stine et al. (2009) applied a ''seasonal response index'' in terms of the lag–gain response between local insolation and temperature. They found a phase advance in the annual cycle of surface temperature, which was partly related to changes in the northern annular mode. Christidis et al. (2007) examined the global and regional changes in the growing season length (GSL) using a temperature-based index. To study overall changes in GSL and its beginning and ending days across regions, local thresholds (annual mean temperatures) were applied at each grid point rather than using a fixed absolute temperature threshold. They detected anthropogenic influences on the lengthened GSL in the NH and Australia associated with earlier onset of spring rather than later start of winter. The faster change in spring onset than in winter start was suggested to be linked to the snow feedback (Groisman et al. 1994; Cayan et al. 2001).

With global warming, the characteristics of each season have changed, inducing associated changes in the characteristics of extreme weather phenomena (Katz and Brown 1992; Bell et al. 2004). In this context, Peña-Ortiz et al. (2015) studied changes in summer season length in Europe, where heatwaves were expected to be more frequent, persistent, and intensified (Barriopedro et al. 2011). They examined changes in summer season length and timing by applying an objective algorithm, and analyzed the effects of global warming and multidecadal variability focusing on the Atlantic multidecadal oscillation (AMO). Results showed that the significant lengthening of European summers was due to combined influences of the global warming and the AMO (cf. Wu et al. 2011; Gao et al. 2015). However, few studies have evaluated the overall observed changes in summer season length and timing across the entire extratropical NH.

Building on the findings of previous studies, we have conducted a systematic analysis of the observed long-term variations in summer season timing and length over land of the NH and its subregions during the past 60 years (1953–2012). We first devised an objective algorithm based on the previous GSL studies, which enables one to determine relative measures of summer onset, withdrawal, and duration at each location. Then, contributions of anthropogenic and natural factors to the observed trends in summer season characteristics were investigated through comparisons with multimodel simulations integrated with different external forcings. Furthermore, we have evaluated the possible contributions of multidecadal variabilities with a focus on regional trends. This study provides the first quantitative assessment of the observed changes in summer season length in the NH.

2. Data and methods

a. Observations and model data

Observations of daily mean temperatures over land in the NH were obtained from the Hadley Centre's Global Historical Climatology Network Daily (HadGHCND; Caesar et al. 2006) datasets for the period of 1953–2012. Gridded data of daily maximum and minimum temperatures were provided with a resolution of 3.75° longitude × 2.5° latitude. We estimated daily mean temperature as the mean of daily maximum and minimum temperatures before calculating the summer season indices (see below). The analysis domain includes extratropical areas north of 23.5°N where a distinct annual cycle occurs (cf. Christidis et al. 2007).

Multimodel simulation datasets were obtained from phase 5 of the Coupled Model Intercomparison Project (CMIP5) experiments (Taylor et al. 2012), which were carried out under the observed external forcings. Three experiments available for the analysis period (1953–2012) were used to compare with observed results: 1) natural (solar plus volcanic activities) plus anthropogenic (greenhouse gases and aerosols emissions) forcing runs (hereafter ALL, 24 models) constructed by merging historical simulations (1953–2005) with future projections based on the representative concentration pathways (RCP) 4.5 scenario (2006–12); 2) greenhouse gas only forcing (hereafter GHG, 6 models); and 3) natural only forcing (hereafter NAT, 8 models). A list of the model simulations used in this study is provided in Table 1. We have evaluated model skills for the climatology of summer season indices and examined its possible influence on the summer season expansion trends (see below).

All model data were interpolated to the same resolution as the observations (hereafter OBS) with the same spatial data coverage being applied. Note that

TABLE 1. List of CMIP5 models and experiments. Number of ensemble members for each model is shown for ALL, GHG, and NAT experiments and the total number of models is shown for each experiment. Asterisks indicate seven skillful models selected based on mean bias and Taylor skill scores. (See text for details.)

	Model	ALL	GHG	NAT
1	ACCESS1–0*	1	—	—
2	ACCESS1–3	1	3	3
3	BCC-CSM-1–1-m	1	—	—
4	BNU-ESM	1	—	—
5	CanESM2*	3	5	5
6	CCSM4*	3	—	—
7	CNRM-CM5	1	5	6
8	CSIRO-Mk3–6-0	9	10	10
9	EC-EARTH*	1	—	—
10	GFDL-CM3	2	—	—
11	GISS-E2-R*	1	—	—
12	HadCM3	9	—	—
13	HadGEM2-AO	1	—	—
14	HadGEM2-ES	2	4	4
15	INMCM4	1	—	—
16	IPSL-CM5A-LR	3	4	3
17	IPSL-CM5A-MR	1	—	3
18	MIROC4h	2	—	—
19	MIROC5	3	—	—
20	MIROC-ESM	1	—	—
21	MPI-ESM-LR*	3	—	—
22	MPI-ESM-MR*	3	—	—
23	MRI-CGCM3	1	—	–
24	NorESM1-M	1	—	1
Total	Model (run)	24 (55)	6 (31)	8 (35)

models can have different land sea mask from the observations, particularly along the coast. When testing sensitivity to the use of each model's land mask, main results based on regional averages remained unaffected (not shown). For models, daily mean temperatures were used, which were found to be very similar to averages of daily maximum and minimum temperatures.

b. Summer season indices

Summer season indices were defined based on a relative threshold that is applied for each grid, following the method of Christidis et al. (2007) used for GSL. To reduce the influence of day-to-day temperature fluctuations, the daily temperature data were first smoothed by applying a third-degree polynomial for each grid box where no data were missing for the given year. The temperature threshold for the summer season was defined as the 75th percentile of temperature values averaged over 1953–2012 (i.e., ''the warmest quarters of the year'') (Trenberth 1983). The spatial distribution of local temperature thresholds in the NH land areas is shown in Fig. 1b. Clear dependency on latitudes with lower thresholds for higher latitudes is revealed by the latitudinal profile of the zonal mean. Summer onset is defined as the calendar date when the smoothed temperature curve begins to exceed the local temperature threshold, and summer withdrawal is defined as the date when the temperature decreases below that threshold. Summer duration is defined simply as the number of days from summer onset to summer withdrawal (Fig. 1a). Hereafter, summer onset, withdrawal and duration are referred to as ''summer season indices.''

To verify that our algorithm is reasonable, sensitivity tests to the use of different threshold criteria and smoothing methods were conducted. To evaluate the suitability of local thresholds, we compared the summer season indices obtained from our algorithm with those from different percentile thresholds (the 70th and 80th percentiles) and an absolute threshold of a daily maximum temperature of 25°C [summer day criterion of Klein Tank and Können (2003)]. The third-degree polynomial fitting was also compared with those obtained from a Butterworth filter and a harmonic function (cf. Qian et al. 2011). Although actual dates of summer season can be somewhat different across filtering methods, both the spatial patterns of the climatology and the trends of summer season indices were largely similar between our results and the results using different thresholds and filtering methods (not shown), indicating the reasonability of the applied threshold and fitting method.

c. Attribution analysis

To identify causes of the observed changes in summer season indices, we estimated contributions of external forcing and natural variability to the observed trends in the NH and its subregions. The long-term natural variability of the ocean may affect the decadal variability of land temperatures by inducing regime shifts such as the AMO and Pacific decadal oscillation (PDO). For this study, the AMO index was calculated as North Atlantic area mean sea surface temperature anomalies using HadISST dataset (Rayner et al. 2003). Many recent studies suggested that the AMO may contain forced responses during recent decades (Gao et al. 2015; Vecchi et al. 2017, and references therein). To isolate the internally driven variability of AMO, we removed global mean sea surface temperature from the original AMO time series following Trenberth and Shea (2006). The PDO index was obtained from the Joint Institute for the Study of the Atmosphere and Ocean (JISAO; Mantua et al. 1997). The monthly data were averaged over each summer season (June–July–August–September (JJAS)]. Although they show different phase transitions during the analysis period (1953–2012) with a positive–negative–positive transition for AMO and a negative–positive–negative transition for PDO, both

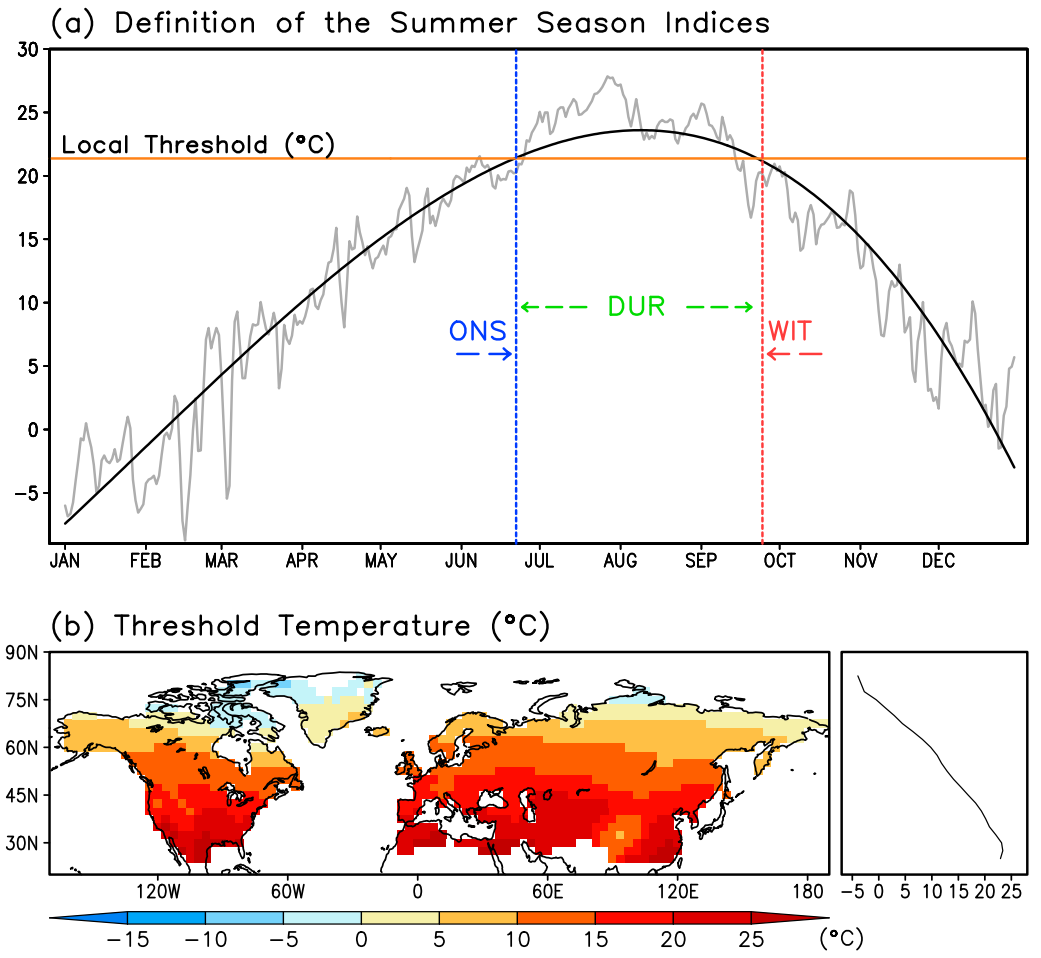

FIG. 1. (a) Schematic illustrating the definitions of the summer season indices (onset, withdrawal, and duration). The horizontal line corresponds to the local temperature threshold (75th percentile). (b) The spatial distribution of local temperature thresholds across the Northern Hemisphere. Zonal mean distribution is displayed on the right.

AMO and PDO exhibit a weak positive trend for the 60 years, potentially contributing to the observed trend in summer season indices.

We employed a stepwise regression method to determine the relative contributions of external forcing and oceanic variability on regional summer season indices following Paik et al. (2017). We calculated 5-yr means over the analysis period to reduce interannual variability noise. As the term suggests, the stepwise regression method involves calculation of each linear regression in a series of steps. First, the following equation is calculated:

$$Y_{\mathrm{OBS}} = \beta_1 X_{\mathrm{ALL}} + \varepsilon, \tag{1}$$

where Y_{OBS} is the observed area-averaged time series of the summer season index, X_{ALL} is the multimodel mean (ALL forcing runs) of the area-averaged time series of the summer season index, β_1 is the regression coefficient, and ε is the residual. The residual represents the observed changes without (anthropogenic plus natural) external forcing, which therefore indicates the internal variability. Another simple linear regression onto the climate variability index (AMO or PDO index here) is then taken to estimate its contribution to the residual as follows:

$$\varepsilon = \beta_2 X_{\mathrm{index}} + \alpha, \tag{2}$$

where the X_{index} denotes either the observed AMO or PDO index, β_2 is the regression coefficient, and the residual of this equation is denoted by α.

To determine the proportion of the observed trend attributable to ALL forcing (C1), linear trends of the

regressed term [$\Delta(\beta_1 X_{\mathrm{ALL}})$] were divided by the linear trend of the observed summer season indices (ΔY_{OBS}):

$$\mathrm{C1} = \frac{\Delta(\beta_1 X_{\mathrm{ALL}})}{\Delta Y_{\mathrm{OBS}}}. \quad (3)$$

Similarly, the proportion of the trend attributable to the climate variability index X_{index} (C2) was calculated as

$$\mathrm{C2} = \frac{\Delta(\beta_2 X_{\mathrm{index}})}{\Delta Y_{\mathrm{OBS}}}. \quad (4)$$

For example, if the AMO index is selected as X_{index}, the trend attributable to AMO can be obtained. This method is also applied to the PDO index. Note that this quantification of contributions to the observed trend was conducted only when the observed trend (ΔY_{OBS}) was statistically significant at the 5% level (see below). This is because weak trends can induce relatively large uncertainty in the denominator in Eqs. (3) and (4), producing unreliable estimates of the contribution.

Next, we assessed significance of the estimated contributions of ALL forcing and AMO or PDO to the observed trends using a method used by Paik et al. (2017). The main idea here is to utilize each model run (ALL forcing runs) as pseudo observations because each model run, not multimodel mean, is comparable to the observations as single realization. For each pseudo observation, we estimated the contributions of ALL and AMO/PDO in the same way as we did for the observations. More specifically, we repeated the procedure from Eq. (1) to Eq. (4) using each ALL forcing run and estimated trends attributable to ALL forcing (C1) and to each type of the simulated multidecadal oceanic variability (C2). Here the only difference is that multimodel mean for ALL runs is calculated excluding the selected run and that the AMO or PDO index defined from the selected run is used. After repeating this calculation across all model runs, we then assessed the 5%–95% uncertainty ranges of C1 and C2. This way of estimating uncertainty ranges is basically identical to those employed in the formal detection and attribution methods (e.g., Allen and Stott 2003). This analysis was conducted for three summer season indices averaged over the whole NH and its subregions.

3. Results

a. Observed changes

The climatological means of the summer season indices exhibited distinct spatial patterns, as shown in Fig. 2. On average, summer started on 15 June and ended on 13 September in the NH. Summer began and ended earlier inland than in coastal areas, from early June to early September and late June to late September, respectively. Strong coastal–inland contrast was identified across the entire NH without notable latitudinal contrast. Stine et al. (2009) suggested that the dominant land–sea contrast in the mean annual cycle can be due to large ocean thermal masses. Many studies have also indicated that the great heat capacity of the ocean is the mechanism that leads to the delay in seasonal transitions over the ocean (Mann and Park 1996; Dwyer et al. 2012).

Figure 3 shows trend patterns of the three summer season indices from 1953 to 2012. Statistical significance of trends is assessed using the Mann–Kendall trend test that considers serial correlation (Hamed and Ramachandra Rao 1998). In line with global warming, summer onset is advanced and summer withdrawal is delayed, which consequently extends the duration of summer (Fig. 3). On average, summer begins 15 days earlier and ends 10 days later, and summer has lengthened by about 25 days over 60 years. The duration of summer increased more at lower latitudes compared with higher latitudes. Note the very weak trends at high latitudes north of 75°N, which are due to too small a land area.

Unusually, summer duration was slightly shortened in the eastern United States, which is not statistically significant. Annual mean temperature in this region shows a cooling trend during the twentieth century, called the "warming hole" (Pan et al. 2004; Portmann et al. 2009) and many researches were conducted to understand the causes. A link has been suggested with the interdecadal Pacific oscillation (IPO), which is closely related to the PDO (Henley et al. 2015); the positive phase of IPO, associated with warm central equatorial Pacific Ocean, induces low-level moisture convergence over the United States in summer, contributing to the warming hole (Meehl et al. 2012). In addition, the cooling effect of anthropogenic aerosols over the United States may be a cause of the warming hole (Leibensperger et al. 2012).

Based on Qian and Zhang (2015), we used the following spatial domains (Fig. 4a): 1) NH: the entire Northern Hemisphere land areas with the observation data; 2) NH1 and NH2: Northern Hemisphere high (50°–85°N) and midlatitudes (23.5°–50°N), respectively; and 3) the NH1 and NH2 regions divided into six subregions: northern Europe (50°–85°N, 10°W–60°E), the Mediterranean (23.5°–50°N, 10°W–60°E), northern Asia (50°–85°N, 60°E–170°W), East Asia (23.5°–50°N, 60°E–170°W), Canada (50°–85°N, 170°–10°W), and the United States (23.5°–50°N, 170°–10°W).

Figure 4b shows the regional trends of summer season indices. The Mediterranean region exhibits the strongest

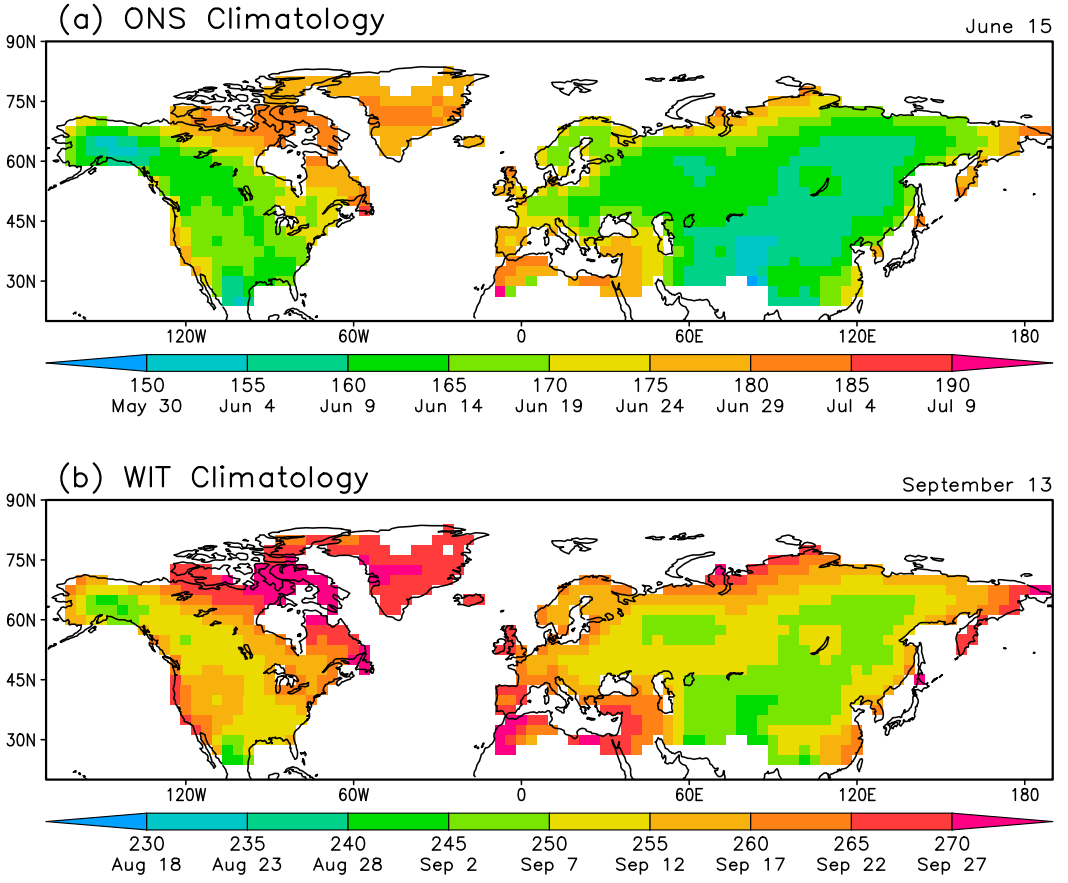

FIG. 2. The spatial patterns of the observed climatology (1953–2012 averages) for (a) summer onset and (b) summer withdrawal in the Northern Hemisphere.

lengthening trends, about 40 days $(60\,\mathrm{yr})^{-1}$ (earliest onset and latest withdrawal), whereas the United States shows the weakest trends, about 12 days $(60\,\mathrm{yr})^{-1}$. Overall, the summer onset trend is stronger than the summer withdrawal trend, which implies that summer duration was extended more by the earlier start than by the delayed ending. This result is similar to previous findings that earlier onset of spring plays a dominant role in the extension of GSL (Menzel and Fabian 1999; Christidis et al. 2007; Song et al. 2010) and also in line with the phase advance in the observed seasonal cycle (Mann and Park 1996; Wallace and Osborn 2002; Stine et al. 2009; Dwyer et al. 2012; Stine and Huybers 2012).

To determine the sensitivity of the summer season indices to temperature change, we examined the relationships between summer season indices and observed monthly temperatures during the summer period (Fig. 5). Overall warming trends during JJAS were significant, except in the eastern United States where a weak negative trend was found as discussed above (Fig. 5a). This pattern is similar to the patterns of summer season index trends (Fig. 3) with spatial correlation coefficients (r_s) greater than 0.7. When examining trend patterns from individual months (not shown), the trend patterns of summer season indices were found to be strongly correlated ($r_s \geq 0.7$) with that of August temperature.

The interannual variability and long-term change of the summer season indices were highly correlated with JJAS mean temperatures on grid scales (Fig. 5b). Temporal correlations (r_t) between summer duration and JJAS mean temperatures were also very strong across the NH land (area mean $r_t > 0.79$), and these relationships were the strongest in the lower latitudes based on both the raw and detrended data. When checking relationship with individual months, summer onset and withdrawal have strong temporal relationships with June and September temperatures, respectively (area mean $r_t > 0.5$). This suggests that the interannual variability and long-term trends of summer onset and withdrawal are sensitive to temperatures of the starting and ending months of summer. On the other hand, summer duration change shows a stronger connection with June temperature on average ($r_t > 0.5$), which seems to be because summer onset advance plays a

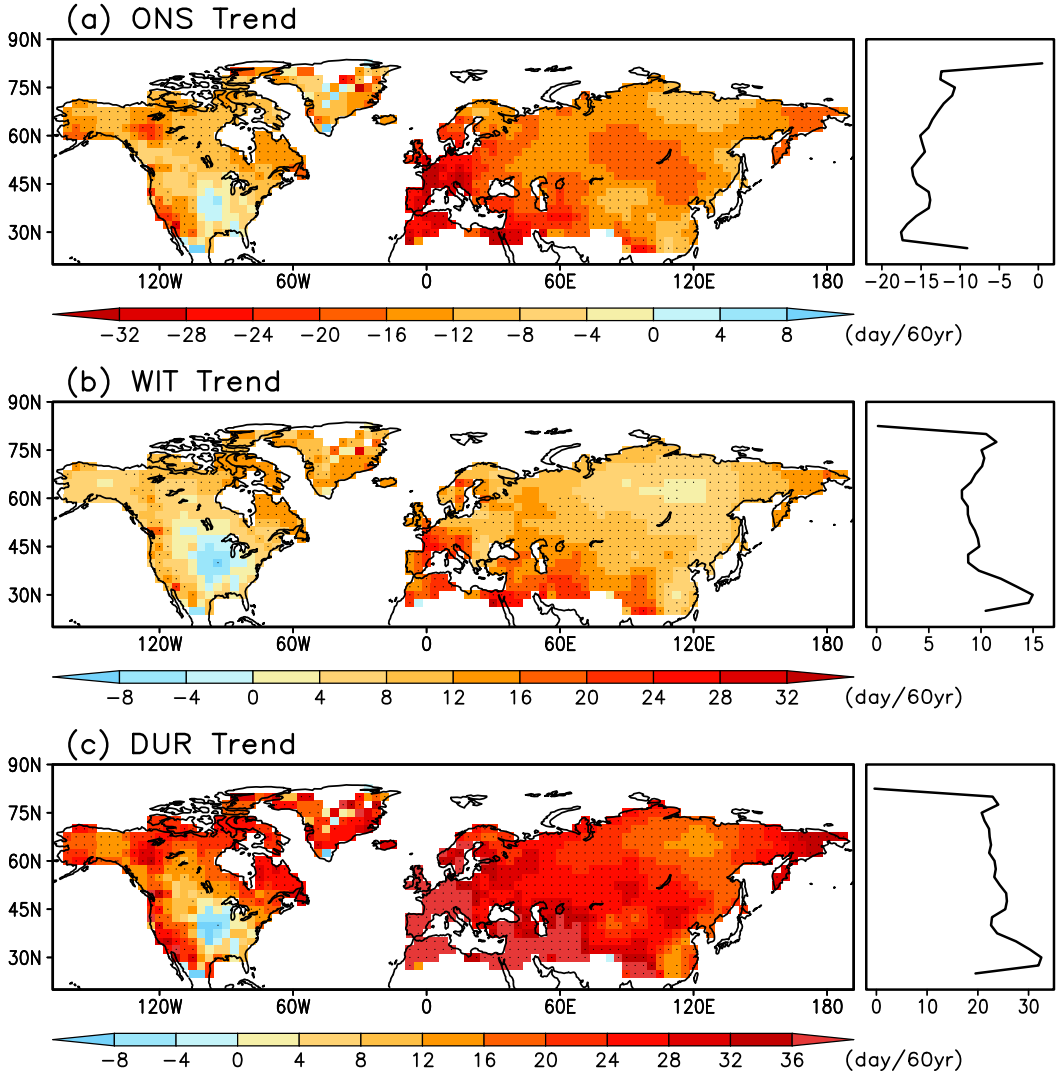

FIG. 3. Spatial distribution of the observed trends in (a) summer onset, (b) summer withdrawal, and (c) summer duration over 1953–2012. The zonal mean trends of the summer season indices are displayed on the right. Dotted grids indicate statistically significant trends at the 5% level based on the Mann–Kendall trend test with serial correlations considered.

major role in summer lengthening in the observations (Fig. 4b).

b. Simulated changes in CMIP5 models

Before examining the impacts of external forcing on the observed summer season indices, we evaluated CMIP5 models (Fig. 6) using bias and the Taylor diagram analysis (Taylor 2001). The ALL experiment of CMIP5 overall reproduces the observed climatological patterns of the summer onset and withdrawal well (Fig. 6). In all models, greater thermal capacity of the ocean caused delayed responses in coastal areas as in the observed. Models, however, tended to have weaker coastal–inland contrast than in the observations. Overall, biases are small within ±2 days, but slightly earlier summer onsets and withdrawals appeared along some coastal areas and Greenland, whereas later starts and ends of summer relative to observations were seen in inland mountain regions (Fig. 6). Individual models can reasonably capture the observed spatial patterns of the summer onset and withdrawal as shown in the Taylor diagrams (Fig. 6). The modeled standard deviations (spatial variability relative to the whole NH area mean) are very similar to the observations, and the spatial correlations range from 0.4 to 0.7 across models for both summer onset and withdrawal indices. In short, CMIP5 models are found to be able to reproduce the observed climatology of summer season indices.

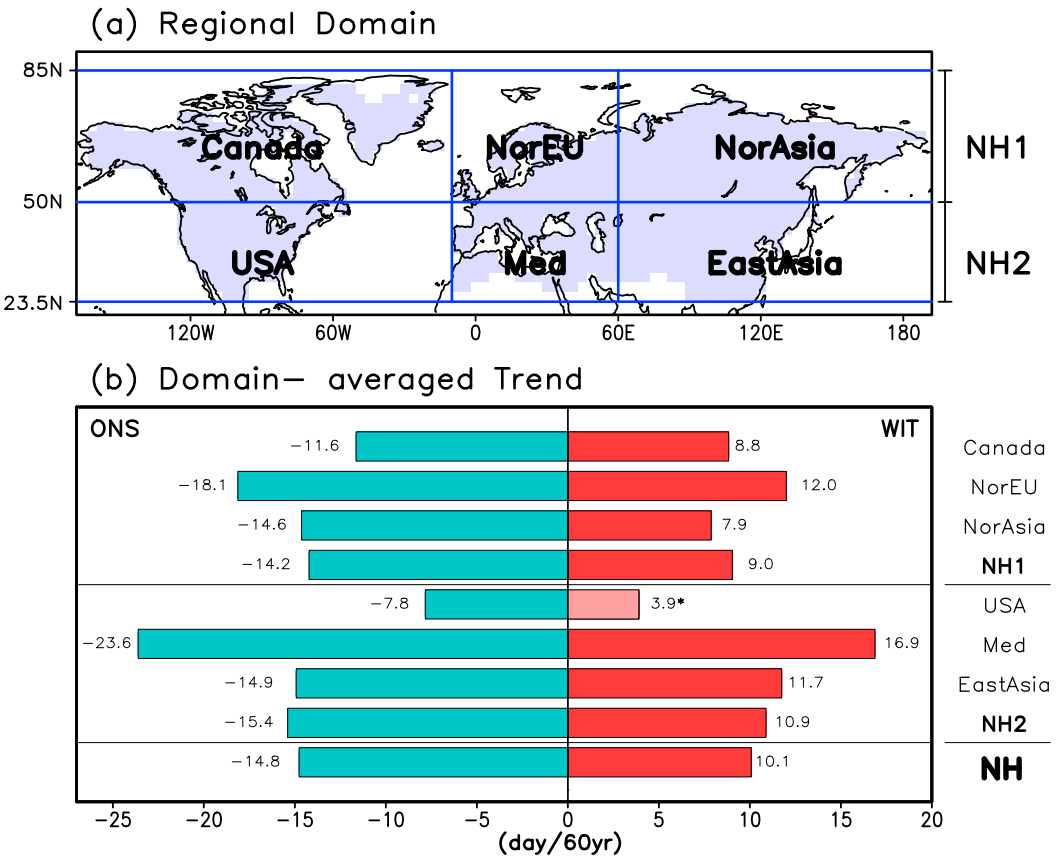

FIG. 4. (a) Regional domains used in this study and abbreviations for the corresponding regions, and (b) regional trends of summer onset (green bar), withdrawal (red bar), and duration (sum of green and red bars); asterisk indicates a statistically insignificant trend.

To find anthropogenic and natural contribution to the observed trend in summer season indices, multimodel mean trend patterns of the summer onset and withdrawal were obtained and compared with the observations (Fig. 7). Generally, ALL produced similar trend patterns to the observations. Slightly weaker trends for summer onset and stronger trends for summer withdrawal were found, resulting in longer durations than the observed change. In the case of GHG, trends patterns of summer season indices are similar to ALL but with stronger amplitude, indicating that anthropogenic forcing due to the GHG increases played a critical role in the summer expansion. In contrast, NAT shows much weaker trends for all summer season indices, representing that natural forcing (solar and volcanic activities) alone cannot explain the observed trend of summer season lengthening during the past 60 years. Even ALL forcing, which showed the most similar spatial distribution to observations, could not accurately reproduce the observed regional characteristics such as the stronger trends in the Europe and the warming hole over the eastern United States. The observation–model differences in regional trends may have been caused in part by the multidecadal variability; AMO was linked to summer lengthening in Europe (Peña-Ortiz et al. 2015), and the IPO likely contributed to the warming hole in the eastern United States as discussed above.

A comparison of the regional trends in summer season indices from ALL, GHG, and NAT experiments with the observed is presented in Fig. 8. ALL forcing (green bars) captured the observed trends of summer onset, withdrawal, and duration well at regional scales, where the multimodel 5%–95% range is positive and covers the observed trend. ALL runs can reproduce the regional differences in the observed rate of summer expansion; for example, the larger increase in the Mediterranean and northern Europe than elsewhere and the larger increase in lower latitudes than in higher latitudes. However, the ALL simulations tend to underestimate the observed trend for summer onset over north Asia, East Asia, and the Mediterranean and overestimate summer withdrawal over most of the regions except the Mediterranean and East Asia. In this regard, Christidis et al. (2007) reported that a CMIP3 model

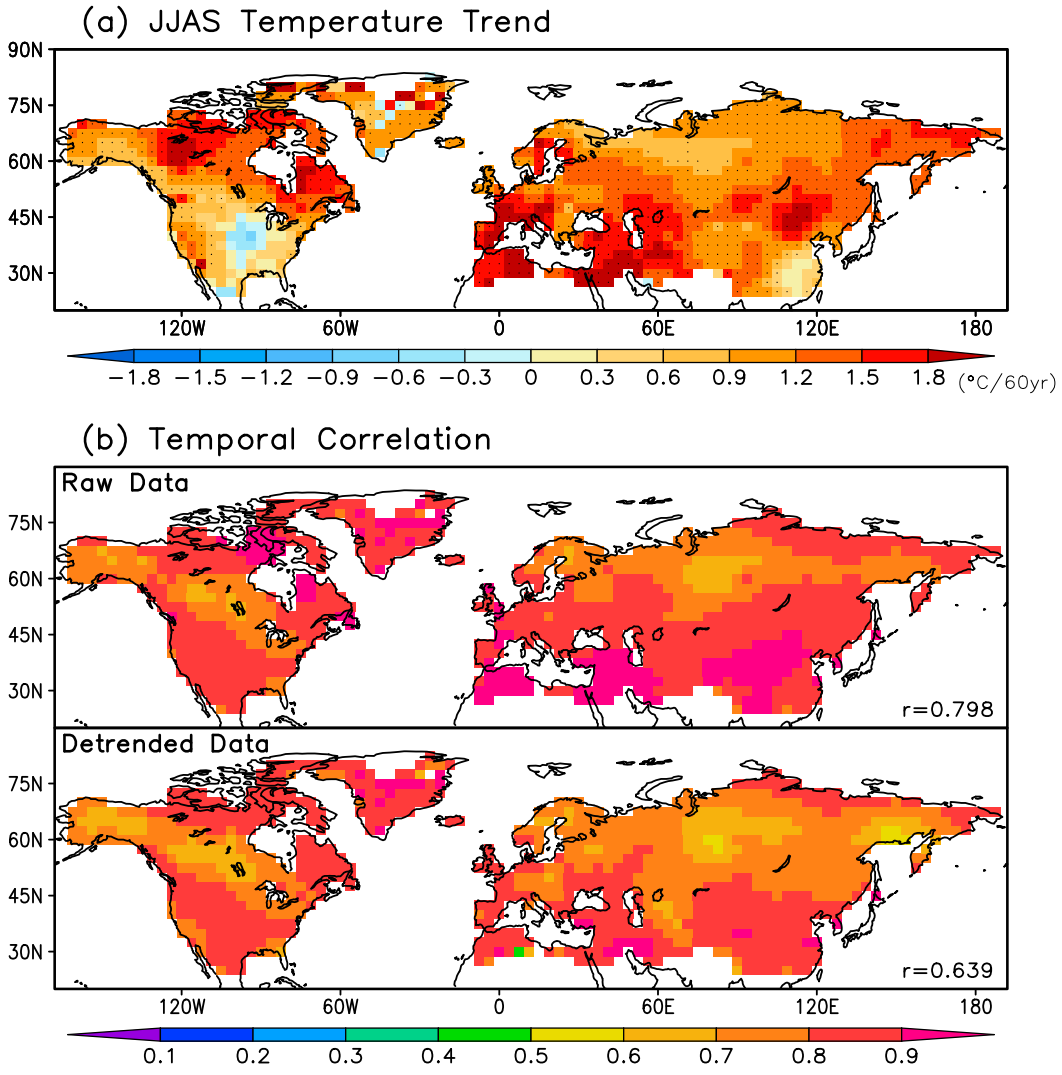

FIG. 5. (a) Spatial patterns of the observed trends in summer mean (JJAS) temperatures where dotted grids indicate statistically significant trends, and (b) spatial distributions of the temporal correlation coefficients between the raw and detrended JJAS temperatures and the summer duration indices over 1953–2012. Area mean correlation values are given in the bottom-right corner.

(HadCM3) tends to underestimate the earlier occurrence of the growing season and suggested that the observation–model differences might be caused by the influence of internal climate variability on the observations, which would not remain in the multimodel means because of the cancellation of different phases of simulated variabilities. GHG (red bars) exhibits stronger trends than ALL over all regions, which indirectly represents the opposite cooling effect of anthropogenic aerosols, which is expected to shorten the summer season length. NAT (blue bars) produces very weak trends in all the summer season indices, compared to ALL and GHG simulations, without explaining the observed changes at all. This qualitative comparison between the observed and simulated regional trends in summer season indices suggest the dominant impact of anthropogenic forcing due to greenhouse gas increases and the negligible impact of natural forcing of solar and volcanic activities on the long-term lengthening trends in summer season indices.

To check robustness of the simulated trends, we examined the influence of model skills on trends in summer season length by repeating our analysis using selected ALL models that can reproduce the observed climatology. From ALL runs, we selected seven skillful models based on bias (less than 2 days) and Taylor skill scores (higher than 0.6, Fig. 6) for both summer onset and summer withdrawal climatology (models marked

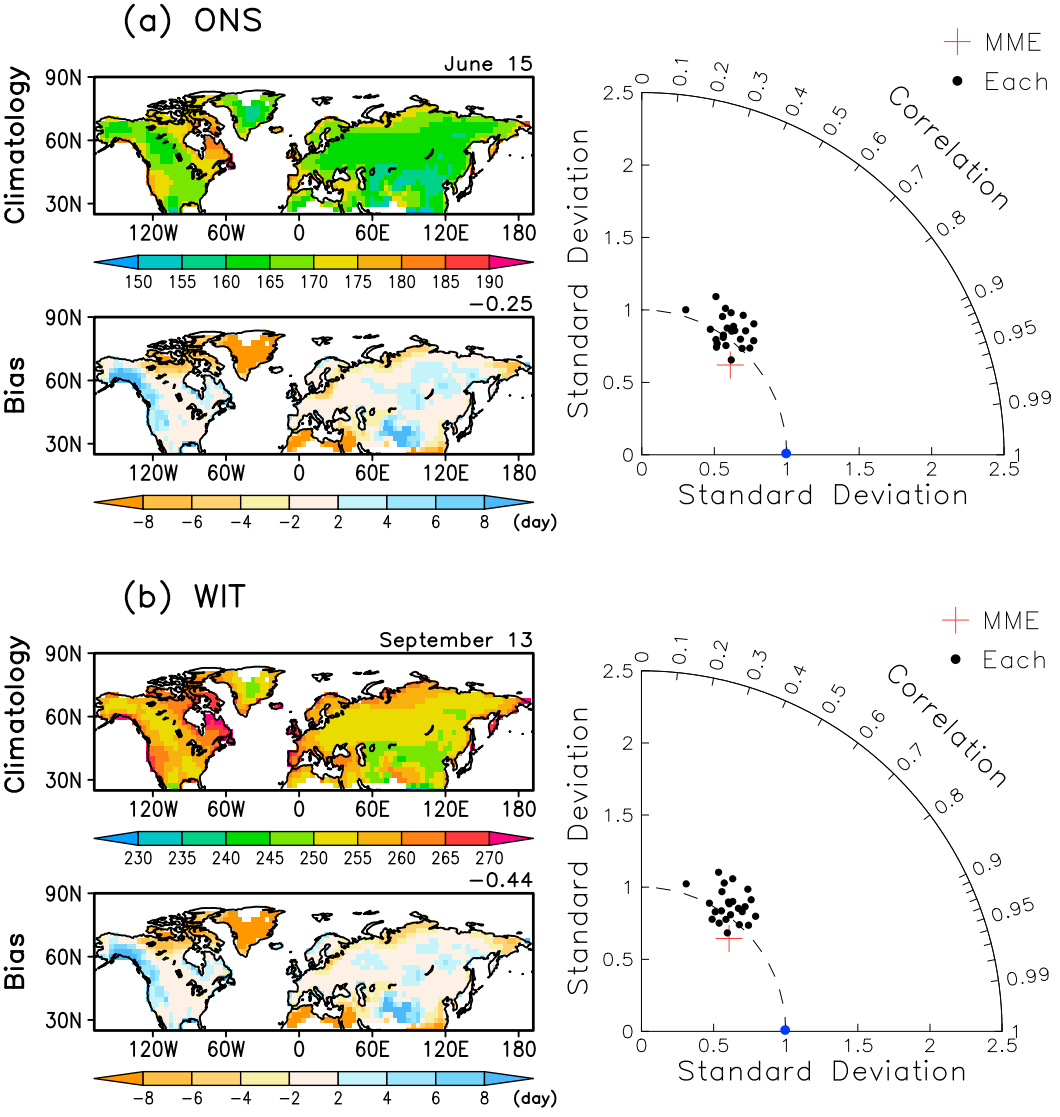

FIG. 6. CMIP5 model skills for (a) summer onset (ONS) and (b) summer withdrawal (WIT) climatology obtained from ALL simulations. Spatial distribution of the multimodel mean (MME) climatology, multimodel mean bias (ALL minus observations), and Taylor diagrams for individual CMIP5 models (black dots) and their MMEs (red cross) in comparison with the observations or a perfect model (blue dot).

with an asterisk in Table 1). The regional trends of these selected models do not show better agreement with observations compared with full-model cases (not shown), which implies that model performance for the climatology of summer season length does not greatly affect the long-term trends.

c. *Forced and internal contributions*

Using the method described in section 2c, attributable trends were obtained for the NH and its subregions (Fig. 9). The United States was omitted from this analysis, where the observed trends in summer season indices were not significant (see above). For most of the summer season indices, ALL forcing contribution [C1 as defined in Eq. (3)] reached around 1, which indicates that most of the observed trends could be explained by external (anthropogenic plus natural) forcing at both continental and regional scales. The proportions of the trends explained by ALL forcing were slightly smaller over the high latitudes for summer onset but larger over Canada and the northern Europe for summer withdrawal (Fig. 9). In all cases, 5%–95% confidence intervals estimated from individual ALL runs (see section 2c) include the contribution of ALL forcing to the observed trend. Relatively large intermodel uncertainties in C1 were found over northern

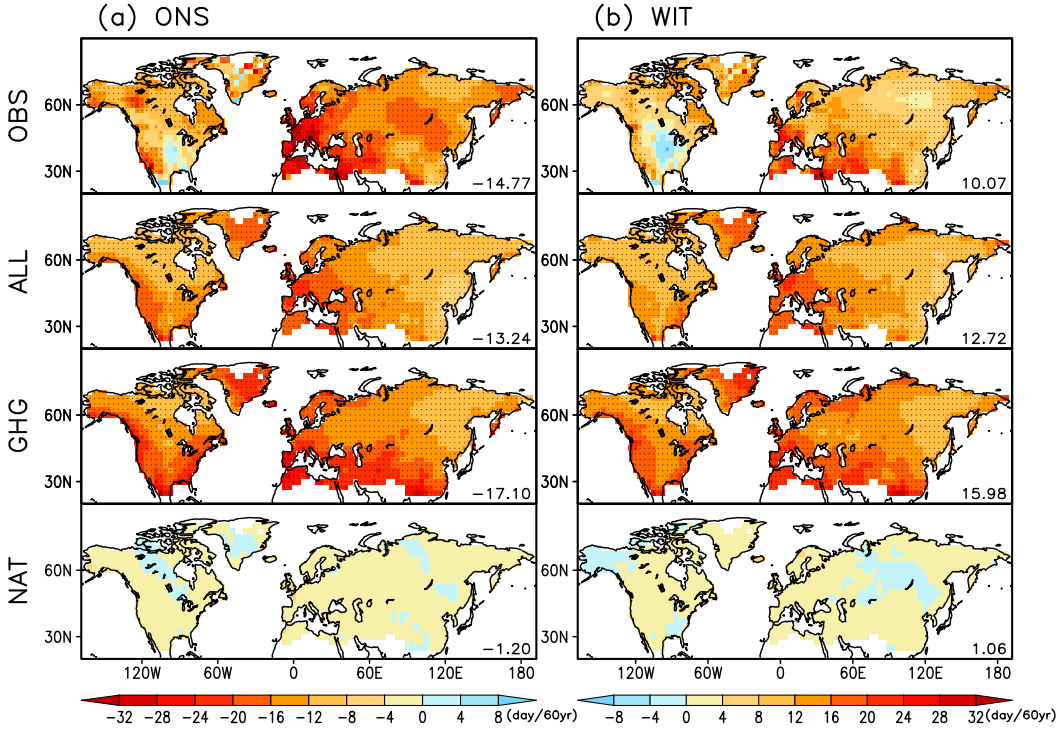

FIG. 7. Spatial distributions of the multimodel mean trends of (a) summer onset and (b) summer withdrawal for ALL, GHG, and NAT experiments. The observed trends (OBS) are displayed again for comparison. Area mean values are given in the bottom-right corner. Dotted grids indicate good intermodel agreement in the sign of trends (more than 80%).

Europe and north Asia, ranging from 0.6 to 1.5 (see below for details).

Although the residual portions of the observed trend were generally not large compared to the forced trends, there might be some contributions of the natural long-term variability to the residual trends in a regional scale. Indeed, when checking correlation between AMO/PDO and residual variations of summer season indices [i.e., the forced portion removed from the raw observation based on Eq. (2)], there were significant correlations over Canada, northern Europe, and the United States, particularly for the summer withdrawal dates (Table 2).

Our attribution results show that in the case of the observed trends in summer onset, weak AMO influence [C2 as defined in Eq. (4)] existed at high latitudes including northern Europe and north Asia, whereas weak PDO influence was found at the midlatitudes such as the Mediterranean and East Asia (Fig. 9a). The contributions from AMO and PDO typically have opposite signs from ALL forcing, meaning that these two modes of decadal to multidecadal climate variabilities provided offsetting effects on the ALL-induced trend of the summer onset advance. The contribution uncertainties estimated from ALL runs included the observed results with C1 ranging from about 0.6 to 1.5 for the ALL contribution and with C2 ranging from around −0.3 to +0.3 for the PDO and AMO contributions. Mixed positive and negative signs of C2 estimated from multiple model simulations suggest the internal origin of the PDO and AMO influences on the summer onset.

For the observed summer withdrawal, ALL contributions were estimated to be near 1. Canada and northern Europe showed the forced contribution larger than 1, which seems to be associated with the overestimated trends by the models (Fig. 8). PDO and AMO impacts were larger on the summer withdrawal than the summer onset over Canada (−7% and +13%, respectively) and northern Europe (−8% and +17%, respectively) where there were stronger correlations of PDO and AMO with the summer withdrawal as shown in Fig. 9 and Table 2. AMO contribution had positive signs, representing the positive contributions to the observed delaying trend in summer withdrawal, while PDO exhibited opposite signs.

Finally, in the results for summer duration, ALL forcing contribution is dominant with C1 values being very close to 1 over all domains. The contributions of AMO and PDO to the observed trend were similar in sign to those for summer withdrawal, but with weaker amplitude. This is likely due to some cancelation between the influences of the two modes of climate variability (AMO and PDO) on summer onset and withdrawal trends, consistent with opposite signs of

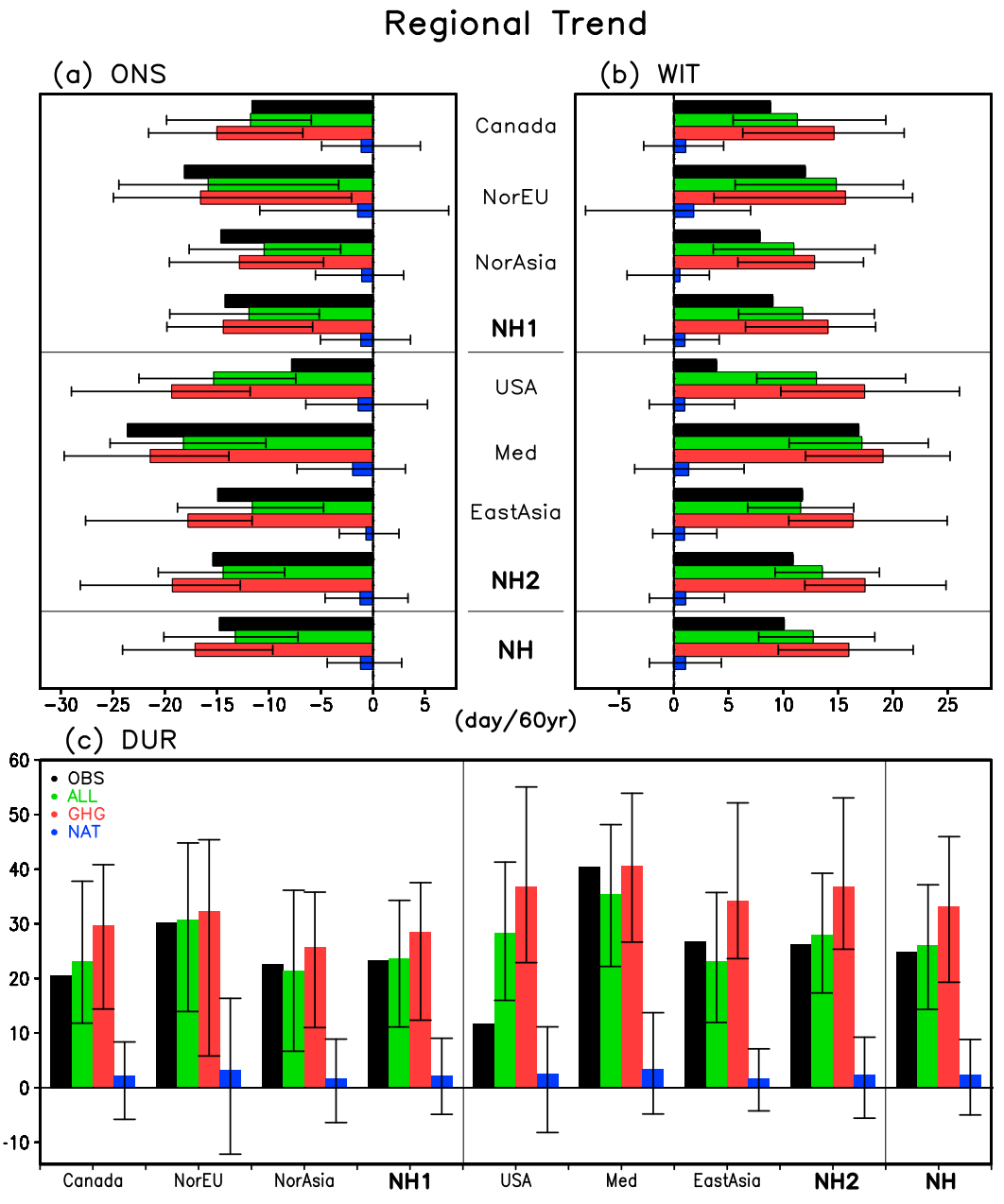

FIG. 8. Domain-averaged trends (days per 60 years) in (a) summer onset, (b) summer withdrawal, and (c) summer duration from observations (black bars), and multimodel means of ALL (green), GHG (red), and NAT (blue bars) experiments. Error bars represent the 5th–95th percentile ranges estimated from individual runs for each experiment.

correlation coefficients in Table 2. The relatively larger gap between OBS and the attributable trends of ALL on summer withdrawal seems to be partly related to the onset–withdrawal contrast in the contribution of the internal climate variability, which warrants further investigation.

d. Asymmetric trends

When the summer duration increases, a symmetric amount of changes in summer onset advance and summer withdrawal delay may be expected. However, based on the overall trends of summer season indices in the NH and its subregions, asymmetric lengthening occurs with the earlier summer onset contributing more to the summer duration extension than does the later summer withdrawal (Fig. 4b). Asymmetry in the seasonal cycle changes related to advance in the onset of spring across the NH has been observed in many studies (Schwartz et al. 2006; Christidis et al. 2007),

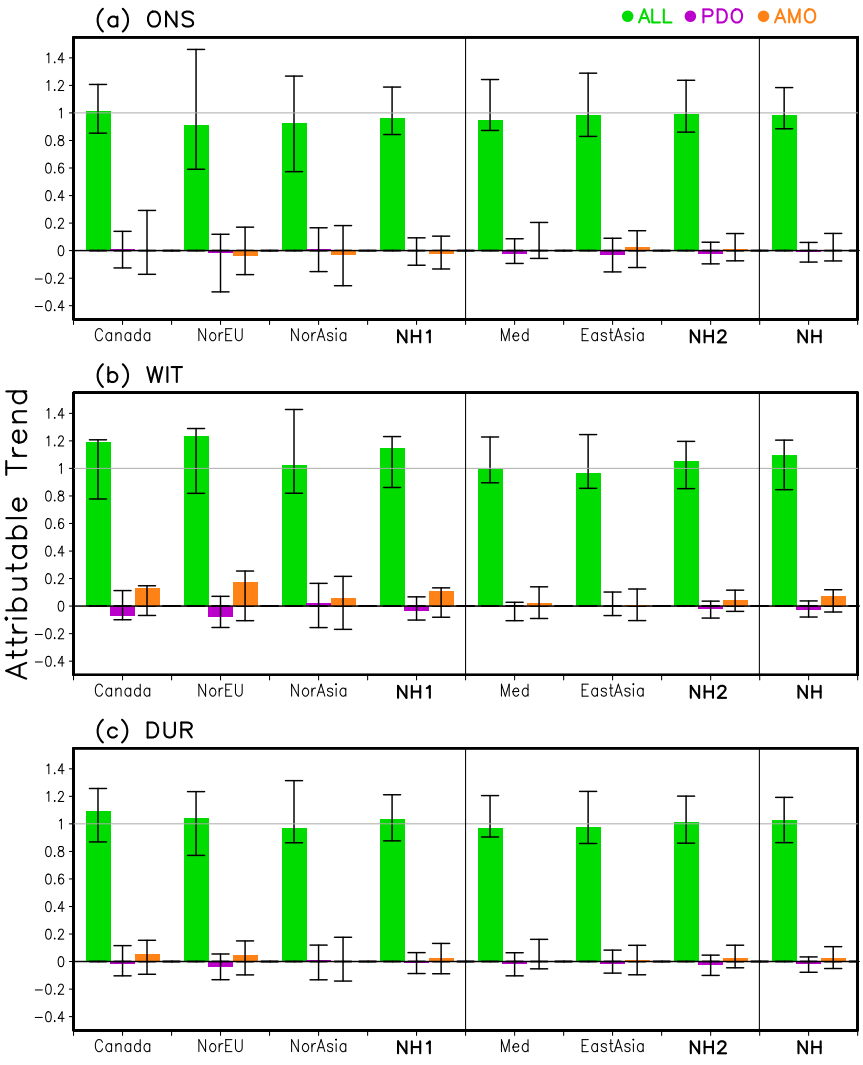

FIG. 9. Attributable trend ratios to the observed total trends [defined as Eqs. (3) and (4)] of ALL forcing (green bars), PDO (purple bars), and AMO (orange bars) for (a) summer onset, (b) summer withdrawal, and (c) summer duration. Error bars indicate 5%–95% ranges of the attributable trend ratios estimated from individual models (see text for details).

possibly linked to the snow feedback (Groisman et al. 1994; Cayan et al. 2001) and the influence of internal climate variability (Christidis et al. 2007). Here, we further check asymmetry observed in the summer season lengthening by comparing observed and simulated spatial patterns of the sum of the trends in summer onset and withdrawal (Fig. 10). Negative signs indicate areas where the trends of change in summer onset are greater than those of withdrawal, and positive signs indicate the reverse. Observations show that earlier summer onset is stronger than delayed withdrawal over the NH lands, except in south Asia, northeast Canada, and Greenland.

Unlike observations, multimodel means of ALL, GHG, and NAT do not reveal significant asymmetry in summer onset and withdrawal trends (Fig. 10). This is consistent with previous studies finding discrepancy in the changes in phases of seasonality although observations and models both indicated decreased amplitude (Mann and Park 1996). The phase delay in the model results in a warmer climate with a scenario of increasing GHG forcing was suggested to be driven by increased effective heat capacity, primarily caused by sea ice loss at high latitudes (Manabe et al. 1992; Mann and Park 1996; Dwyer et al. 2012). ALL and GHG results in our study also exhibit the phase delay at high altitudes as that in the future projections (Fig. 10).

TABLE 2. Correlation coefficients between AMO and PDO indices and residual time series of the summer season onset, withdrawal, and duration for each region. Residual time series (ε) is obtained by removing the forced portion from the raw observations based on linear regression against the ALL results as described in Eq. (2). The 5-yr means are used in this calculation and asterisk (double asterisks) represents significant correlation at the 10% (5%) level based on a t test.

		Canada	Northern Europe	Northern Asia	NH1	United States	Mediterranean	East Asia	NH2	NH
ONS	AMO	−0.008	0.241	0.256	0.244	−0.041	0.031	−0.190	−0.134	0.019
	PDO	−0.197	0.154	−0.137	−0.107	0.158	0.405	0.455	0.633*	0.374
WIT	AMO	0.697**	0.549*	0.227	0.559*	0.619**	0.123	0.035	0.380	0.514
	PDO	−0.698**	−0.445	0.138	−0.348	−0.537*	−0.006	0.008	−0.245	−0.317
DUR	AMO	0.479	0.301	−0.002	0.314	0.562*	0.048	0.153	0.309	0.398
	PDO	−0.341	−0.455	0.197	−0.230	−0.550*	−0.249	−0.373	−0.507	−0.452

The disagreement between multimodel means of the historical simulations and observations may be governed by natural internal variabilities at midlatitudes, which cannot be reflected in the multimodel ensemble mean (Stine et al. 2009; Stine and Huybers 2012). For instance, Stine and Huybers (2012) found that the observed variability in the phase of the annual cycle of surface temperature is most strongly influenced by springtime atmospheric circulation, as represented by the northern annular mode and the Pacific–North America mode. However, they focused on the wintertime phase shift, which is not directly applicable to the asymmetric changes in summer season length. This observation–model inconsistency appears related to the models' underestimation of summer onset advance and overestimation of summer withdrawal delay (Fig. 8), mechanisms for which remain to be determined.

4. Summary and conclusions

The observed long-term changes in the timing and length of the summer season in the NH and its subregions during 1953–2012 were analyzed using temperature-based indices. A revised algorithm based on GSL was developed to identify the timing of the summer season across regions. Based on local temperature thresholds, we defined summer onset, withdrawal, and duration based on the characteristics of each region. In general, summer begins and ends earlier inland, whereas coastal regions experience later onset and withdrawal, which represents the land–ocean differences in heat capacity.

For the period of 1953–2012, observations indicate statistically significant lengthening of the summer season with the advance of summer onset and the delay of summer withdrawal across all land regions of the NH. Regional differences in the summer onset and withdrawal trends were observed with strongest trends over the Mediterranean and weakest trends in the United States. Overall, the trends of summer onset have contributed more to the observed increases in the length of the summer season than the trends of summer withdrawal. In addition, the stronger trends of summer expansion appeared at lower latitudes, which is consistent with the stronger relationship between summer season indices and monthly temperatures over the regions.

To identify the causes of the observed long-term changes, we compared observed summer season trends with those from multimodel CMIP5 simulations under different forcing conditions. The ALL and GHG simulations were found to capture the observed trend patterns of global and regional lengthening of the summer season, but NAT runs showed negligible trends. These indicate that anthropogenic forcing caused primarily by increased greenhouse gas emissions has been the main factor driving the observed lengthening of summer seasons in the NH and its subregions. However, ALL runs tend to underestimate the observed trend of summer onset and overestimate the withdrawal trend. In other words, the models exhibited delayed responses in the phase of seasonal cycle for the Northern Hemisphere land, which was similar to the future phase delay under global warming caused mainly by Arctic sea ice loss (e.g., Dwyer et al. 2012). This is also in agreement with the simulated delay in the summer peak date when maximum temperature occurs during summer, which is opposite to the advance in the observed peak date (not shown).

Using an approach based on a stepwise linear regression, we have quantified the relative contribution of external (ALL) forcing and internal multidecadal variabilities such as the AMO and PDO to the observed trends in summer season timing and length for the NH and its subregions. Uncertainty ranges of the external and internal contributions were estimated from individual model runs. The results show that in all regions, the ALL forcing explains most of the observed lengthening trend of the summer season and that the 5%–95% confidence intervals include the observed results, indicating the robustness of the external contribution. Since, by definition, the summer season length should be closely related to the summer temperature (as shown in Fig. 5), the dominant contributions of ALL forcing to the

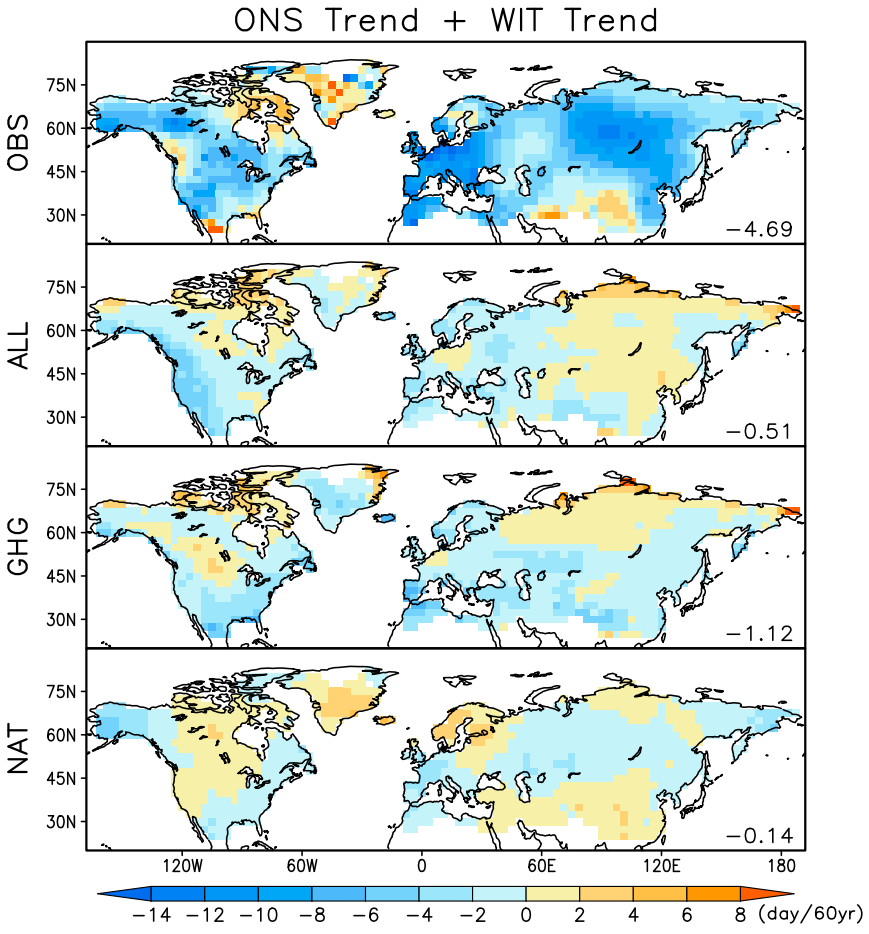

FIG 10. Spatial patterns of the sum of trends in summer onset and withdrawal for the observations (OBS) and multimodel means (ALL, GHG, and NAT experiments).

summer season expansion identified in all regions are physically reasonable. Indeed, this is well consistent with Qian and Zhang (2015) who robustly detected ALL forcing in the observed regional summer temperatures.

PDO and AMO were also found to contribute a moderate amount to the observed trends, about ±10%, depending on the regions and summer season indices. The contribution of AMO was greater than PDO over the high latitudes for the summer withdrawal, which seems to be in part due to the stronger influence of AMO on summer temperature over the NH land. Actual contribution of AMO/PDO to the observed trend in summer season indices will be dependent on temperature responses of the regions to the AMO/PDO and also changes in AMO/PDO phases or trends during the analysis period. Further investigation is needed to explore physical mechanisms of the externally forced and internally generated lengthening of the summer season across regions. Also, causes of the observation–model inconsistency need to be examined, particularly asymmetric trends in the observations (i.e., stronger onset advance than withdrawal delay), which are hardly reproduced by the models.

Acknowledgments. This study was supported by the Korea Meteorological Administration Research and Development Program under Grant KMIPA 2016-6040 and by the National Research Foundation of Korea (NRF) grant funded by the Ministry of Science and ICT (Grant 2017R1A2B2008951). We acknowledge the World Climate Research Programme's Working Group on Coupled Modelling, which is responsible for CMIP, and we thank the climate modeling groups (listed in Table 1 of this paper) for producing and making available their model output. The authors are grateful to Drs. Wasyl Drosdowsky, Linden Ashcroft, and Robert Colman at the Australian Bureau of Meteorology and two anonymous reviewers for their constructive comments on the manuscript.

REFERENCES

Allen, M. R., and P. A. Stott, 2003: Estimating signal amplitudes in optimal fingerprinting, part I: Theory. *Climate Dyn.*, **21**, 477–491, https://doi.org/10.1007/s00382-003-0313-9.

Barriopedro, D., E. M. Fisher, J. Luterbacher, R. M. Trigo, and R. García-Herrera, 2011: The hot summer of 2010: Redrawing the temperature record map of Europe. *Science*, **332**, 220–224, https://doi.org/10.1126/science.1201224.

Bell, J. L., L. C. Sloan, and M. A. Snyder, 2004: Regional changes in extreme climatic events: A future climatic scenario. *J. Climate*, **17**, 81–87, https://doi.org/10.1175/1520-0442(2004)017<0081:RCIECE>2.0.CO;2.

Bertram, D. F., D. L. Mackas, and S. M. McKinnell, 2001: The seasonal cycle revisited: Interannual variation and ecosystem consequences. *Prog. Oceanogr.*, **49**, 283–307, https://doi.org/10.1016/S0079-6611(01)00027-1.

Caesar, J., L. Alexanderm, and R. Vose, 2006: Large-scale changes in observed daily maximum and minimum temperatures: Creation and analysis of a new gridded data set. *J. Geophys. Res.*, **111**, D05101, https://doi.org/10.1029/2005JD006280.

Cayan, D. R., S. A. Kammerdiener, M. D. Dettinger, J. M. Caprio, and D. H. Peterson, 2001: Changes in the onset of spring in the western United States. *Bull. Amer. Meteor. Soc.*, **82**, 399–415, https://doi.org/10.1175/1520-0477(2001)082<0399:CITOOS>2.3.CO;2.

Christidis, N., D. J. Karoly, and J. Caesar, 2007: Human contribution to the lengthening of the growing season during 1950–99. *J. Climate*, **20**, 5441–5454, https://doi.org/10.1175/2007JCLI1568.1.

Cornes, R., P. Jones, and C. Qian, 2017: Twentieth-century trends in the annual cycle of temperature across the Northern Hemisphere. *J. Climate*, **30**, 5755–5773, https://doi.org/10.1175/JCLI-D-16-0315.1.

Dwyer, J. G., M. Biasutti, and A. H. Sobel, 2012: Projected changes in the seasonal cycle of surface temperature. *J. Climate*, **25**, 6359–6374, https://doi.org/10.1175/JCLI-D-11-00741.1.

Gao, L. H., Z. W. Yan, and X. W. Quan, 2015: Observed and SST-forced multidecadal variability in global land surface air temperature. *Climate Dyn.*, **44**, 359–369, https://doi.org/10.1007/s00382-014-2121-9.

Groisman, P. Ya., T. P. Karl, and R. W. Knight, 1994: Observed impact of snow cover on the heat balance and the rise of continental spring temperature. *Science*, **263**, 198–200, https://doi.org/10.1126/science.263.5144.198.

Hamed, K. H., and A. Ramachandra Rao, 1998: A modified Mann–Kendall trend test for autocorrelated data. *J. Hydrol.*, **204**, 182–196, https://doi.org/10.1016/S0022-1694(97)00125-X.

Henley, B. J., J. Gergis, D. J. Karoly, S. Power, J. Kennedy, and C. K. Folland, 2015: A tripole index for the Interdecadal Pacific Oscillation. *Climate Dyn.*, **45**, 3077–3090, https://doi.org/10.1007/s00382-015-2525-1.

Katz, R. W., and B. G. Brown, 1992: Extreme events in a changing climate: Variability is more important than averages. *Climatic Change*, **21**, 289–302, https://doi.org/10.1007/BF00139728.

Klein Tank, A. M. G., and G. P. Können, 2003: Trends in indices of daily temperature and precipitation extremes in Europe, 1946–99. *J. Climate*, **16**, 3665–3680, https://doi.org/10.1175/1520-0442(2003)016<3665:TIIODT>2.0.CO;2.

Leibensperger, E. M., and Coauthors, 2012: Climatic effects of 1950–2050 changes in US anthropogenic aerosols—Part 2: Climate response. *Atmos. Chem. Phys.*, **12**, 3349–3362, https://doi.org/10.5194/acp-12-3349-2012.

Manabe, S., M. J. Spelman, and R. J. Stouffer, 1992: Transient responses of a coupled ocean–atmosphere model to gradual changes of atmospheric CO_2. Part II: Seasonal response. *J. Climate*, **5**, 105–126, https://doi.org/10.1175/1520-0442(1992)005<0105:TROACO>2.0.CO;2.

Mann, M. E., and J. Park, 1996: Greenhouse warming and changes in the seasonal cycle of temperature: Model versus observations. *Geophys. Res. Lett.*, **23**, 1111–1114, https://doi.org/10.1029/96GL01066.

Mantua, N. J., S. R. Hare, Y. Zhang, J. M. Wallace, and R. C. Francis, 1997: A Pacific interdecadal climate oscillation with impacts on salmon production. *Bull. Amer. Meteor. Soc.*, **78**, 1069–1079, https://doi.org/10.1175/1520-0477(1997)078<1069:APICOW>2.0.CO;2.

Meehl, G. A., J. M. Arblaster, and G. Branstator, 2012: Mechanisms contributing to the warming hole and the consequent U.S. east–west differential of heat extremes. *J. Climate*, **25**, 6394–6408, https://doi.org/10.1175/JCLI-D-11-00655.1.

Menzel, A., and P. Fabian, 1999: Growing season extended in Europe. *Nature*, **397**, 659, https://doi.org/10.1038/17709.

Paik, S., S.-K. Min, Y.-H. Kim, B.-M. Kim, H. Shiogama, and J. Heo, 2017: Attributing causes of 2015 record minimum sea-ice extent in the Sea of Okhotsk. *J. Climate*, **30**, 4693–4703, https://doi.org/10.1175/JCLI-D-16-0587.1.

Pan, Z., R. W. Arritt, E. S. Takle, W. J. Gutowski Jr., C. J. Anderson, and M. Segal, 2004: Altered hydrologic feedback in a warming climate introduces a ''warming hole.'' *Geophys. Res. Lett.*, **31**, L17109, https://doi.org/10.1029/2004GL020528.

Parmesan, C., 2006: Ecological and evolutionary responses to recent climate change. *Annu. Rev. Ecol. Evol. Syst.*, **37**, 637–669, https://doi.org/10.1146/annurev.ecolsys.37.091305.110100.

Peña-Ortiz, C., D. Barriopedro, and R. Garcia-Herrera, 2015: Multidecadal variability of the summer length in Europe. *J. Climate*, **28**, 5375–5388, https://doi.org/10.1175/JCLI-D-14-00429.1.

Portmann, R. W., S. Solomon, and G. C. Hegerl, 2009: Spatial and seasonal patterns in climate change, temperatures, and precipitation across the United States. *Proc. Natl. Acad. Sci. USA*, **106**, 7324–7329, https://doi.org/10.1073/pnas.0808533106.

Qian, C., and X. Zhang, 2015: Human influences on changes in the temperature seasonality in mid- to high-latitude land areas. *J. Climate*, **28**, 5908–5921, https://doi.org/10.1175/JCLI-D-14-00821.1.

——, C. B. Fu, Z. Wu, and Z. W. Yan, 2011: The role of changes in the annual cycle in earlier onset of climatic spring in northern China. *Adv. Atmos. Sci.*, **28**, 284–296, https://doi.org/10.1007/s00376-010-9221-1.

——, Z. W. Yan, and C. B. Fu, 2012: Climatic changes in the twenty-four solar terms during 1960–2008. *Chin. Sci. Bull.*, **57**, 276–286, https://doi.org/10.1007/s11434-011-4724-4.

Rayner, N. A., D. E. Parker, E. B. Horton, C. K. Folland, L. V. Alexander, D. P. Rowell, E. C. Kent, and A. Kaplan 2003: Global analyses of sea surface temperature, sea ice, and night marine air temperature since the late nineteenth century. *J. Geophys. Res.*, **108**, 4407, https://doi.org/10.1029/2002JD002670.

Schwartz, M. D., R. Ahas, and A. Aasa, 2006: Onset of spring starting earlier across the Northern Hemisphere. *Global Change Biol.*, **12**, 343–351, https://doi.org/10.1111/j.1365-2486.2005.01097.x.

Song, Y., H. W. Linderholm, D. Chen, and A. Walther, 2010: Trends of the thermal growing season in China, 1951–2007. *Int. J. Climatol.*, **30**, 33–43, https://doi.org/10.1002/joc.1868.

Stine, A. R., P. Huybers, and I. Y. Fung, 2009: Changes in the phase of the annual cycle of surface temperature. *Nature*, **457**, 435–440, https://doi.org/10.1038/nature07675.

——, and ——, 2012: Changes in the seasonal cycle of temperature and atmospheric circulation. *J. Climate*, **25**, 7362–7380, https://doi.org/10.1175/JCLI-D-11-00470.1.

Taylor, K. E., 2001: Summarizing multiple aspects of model performance in a single diagram. *J. Geophys. Res.*, **106**, 7183–7192, https://doi.org/10.1029/2000JD900719.

——, R. J. Stouffer, and G. A. Meehl, 2012: An overview of CMIP5 and the experiment design. *Bull. Amer. Meteor. Soc.*, **93**, 485–498, https://doi.org/10.1175/BAMS-D-11-00094.1.

Trenberth, K. E., 1983: What are the seasons? *Bull. Amer. Meteor. Soc.*, **64**, 1276–1277, https://doi.org/10.1175/1520-0477(1983)064<1276:WATS>2.0.CO;2.

——, and D. J. Shea, 2006: Atlantic hurricanes and natural variability in 2005. *Geophys. Res. Lett.*, **33**, L12704, https://doi.org/10.1029/2006GL026894.

Vecchi, G. A., T. L. Delworth, and B. Booth, 2017: Climate science: Origins of Atlantic decadal swings. *Nature*, **548**, 284–285, https://doi.org/10.1038/nature23538.

Wallace, C. J., and T. J. Osborn, 2002: Recent and future modulation of the annual cycle. *Climate Res.*, **22**, 1–11, https://doi.org/10.3354/cr022001.

Walther, R., and Coauthors, 2002: Ecological responses to recent climate change. *Nature*, **416**, 389–395, https://doi.org/10.1038/416389a.

Wu, Z. H., N. E. Huang, J. M. Wallace, B. V. Smoliak, and X. Y. Chen, 2011: On the time-varying trend in global-mean surface temperature. *Climate Dyn.*, **37**, 759–773, https://doi.org/10.1007/s00382-011-1128-8.